

Unified one-dimensional finite element for the analysis of hyperelastic soft materials and structures

Original

Unified one-dimensional finite element for the analysis of hyperelastic soft materials and structures / Pagani, A.; Carrera, E.. - In: MECHANICS OF ADVANCED MATERIALS AND STRUCTURES. - ISSN 1537-6494. - STAMPA. - 30:2(2023), pp. 342-355. [10.1080/15376494.2021.2013585]

Availability:

This version is available at: 11583/2947806 since: 2023-02-01T09:02:57Z

Publisher:

Taylor & Francis

Published

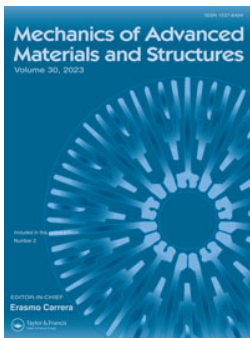
DOI:10.1080/15376494.2021.2013585

Terms of use:

This article is made available under terms and conditions as specified in the corresponding bibliographic description in the repository

Publisher copyright

(Article begins on next page)



Unified one-dimensional finite element for the analysis of hyperelastic soft materials and structures

A. Pagani & E. Carrera

To cite this article: A. Pagani & E. Carrera (2023) Unified one-dimensional finite element for the analysis of hyperelastic soft materials and structures, *Mechanics of Advanced Materials and Structures*, 30:2, 342-355, DOI: [10.1080/15376494.2021.2013585](https://doi.org/10.1080/15376494.2021.2013585)

To link to this article: <https://doi.org/10.1080/15376494.2021.2013585>



© 2021 The Author(s). Published with license by Taylor & Francis Group, LLC



Published online: 23 Dec 2021.



Submit your article to this journal [↗](#)



Article views: 1630



View related articles [↗](#)



View Crossmark data [↗](#)



Citing articles: 6 View citing articles [↗](#)

Unified one-dimensional finite element for the analysis of hyperelastic soft materials and structures

A. Pagani  and E. Carrera

Mul² Lab Department of Mechanical and Aerospace Engineering, Politecnico di Torino, Torino, Italy

ABSTRACT

Based on the Carrera unified formulation (CUF) and first-invariant hyperelasticity, this work proposes a displacement-based high order one-dimensional (1D) finite element model for the geometrical and physical nonlinear analysis of isotropic, slightly compressible soft material structures. Different strain energy functions are considered and they are decomposed in a volumetric and an isochoric part, the former acting as penalization of incompressibility. Given the material Jacobian tensor, the nonlinear governing equations are derived in a unified, total Lagrangian form by expanding the three-dimensional displacement field with arbitrary cross-section polynomials and using the virtual work principle. The exact analytical expressions of the elemental internal force vector and tangent matrix of the unified beam model are also provided. Several problems are addressed, including uniaxial tension, bending of a slender structure, compression of a three-dimensional block, and a thick pinched cylinder. The proposed model is compared with analytical solutions and literature results whenever possible. It is demonstrated that, although 1D, the present CUF-based finite element can address simple to complex nonlinear hyperelastic phenomena, depending on the theory approximation order.

ARTICLE HISTORY

Received 29 November 2021
Accepted 29 November 2021

KEYWORDS

High-order finite elements; beams; soft matter; nearly incompressible hyperelastic materials; first-invariant hyperelasticity



1. Introduction

Structures made of hyperelastic soft materials, such as elastomers and gels, can undergo extreme stretching before failure occurs. They are intrinsically compliant at the constitutive level and have unique elastic characteristics that can be exploited to produce functional devices; e.g. flexible pressure sensors [1], soft optical composites for tunable transmittance [2], electro-active tunable devices [3], etc.

Being the bulk modulus order of magnitudes larger than the shear modulus [4], the nonlinear finite element analysis of nearly incompressible hyperelastic materials offers many challenges though. The main causes are volumetric locking and hourglass instability resulting as a consequence of ill-conditioned stiffness matrices [5]. Over the last decades, many researches have addressed these difficulties. Classical works explored the application of mixed methods for dealing with the incompressibility constraint in the nonlinear regime [6, 7]. Many later works were based on the seminal idea of Simo and Armero [8], who derived a pure displacement formulation with no volumetric locking by using static condensation and introducing incompatible modes and other enhancement functions within a Hu–Washizu mixed formulation, see the work of Caylak and Mahnken [9] for example. This paper and several others in the literature (e.g. [10]) rely, instead, on the \bar{F} method [11], based on a local multiplicative split of the deformation gradient into volume-preserving and dilatational parts.

Although the aforementioned techniques have met with success for simulating hyperelasticity and elasto-plasticity by plain-strain quadrilateral and solid finite elements (FEs), the need to develop simple but effective models for soft beam, plate and shell structures able to overcome the issues associated with the computational burdensome of some problems of practical interest is fairly clear. However, Antman and Schuricht [12] demonstrated that it is very complex to formulate rod and shell theories that exactly preserve the incompressibility. A brief overview of available theories for one-dimensional (1D) and two-dimensional (2D) soft structures is given in the following anyhow for the sake of completeness.

Quite recently, Attard [13] provided a comprehensive review of finite-strain beam theories. Chen and Wang [14] derived the governing equations of Yeoh hyperelastic soft beams by using the inextensibility assumption of the beam's centerline and the principle of minimum potential energy. Lubbers *et al.* [15] studied the sub-critical buckling of neo-Hookean wide beams by developing a 1D nonlinear beam model by combining the Reissner-Mindlin kinematics with a nonlinearity in the stress-strain relation. A similar problem was also considered by Chen and Jin [16]. Breslavsky *et al.* [17] analyzed static deformations and free and forced nonlinear vibrations of thin rectangular plates made of incompressible neo-Hookean material. The classical von Kàrmàn nonlinear plate theory was used and the transverse normal

CONTACT A. Pagani  alfonso.pagani@polito.it  Mul² Lab Department of Mechanical and Aerospace Engineering, Politecnico di Torino Corso Duca degli Abruzzi 24, 10129 Torino, Italy.

© 2021 The Author(s). Published with license by Taylor & Francis Group, LLC

This is an Open Access article distributed under the terms of the Creative Commons Attribution-NonCommercial-NoDerivatives License (<http://creativecommons.org/licenses/by-nc-nd/4.0/>), which permits non-commercial re-use, distribution, and reproduction in any medium, provided the original work is properly cited, and is not altered, transformed, or built upon in any way.

strain was obtained from the incompressibility condition. Breslavsky *et al.* [18] then extended this study to Mooney–Rivlin as well as Ogden hyperelastic laws. Rectangular plates made of isotropic or anisotropic, linearly elastic incompressible material were studied through opportune analytical solutions by Aimmanee and Batra [19]. Amabili *et al.* [20] investigated the hyperelastic behavior of a thin square silicone rubber plate analytically, numerically and experimentally. In particular, the equations of motions were based on a unified energy approach, whereas the geometrical nonlinearities relied upon the Novozhilov nonlinear shell theory. Later, a higher-order 9-parameter geometrically nonlinear theory for circular cylindrical shells made of incompressible hyperelastic materials was developed by the same author [21]. Pascon and Coda [22] developed a triangular shell FE formulation with seven nodal parameters to analyze highly deformable shell structures composed of homogeneous rubber-like materials.

The proposed study introduces a unified 1D finite element for the analysis of soft material structures. This finite beam element is based on the Carrera Unified Formulation (CUF), which gives the possibility to write the governing equations in a compact form by using a recursive index notation [23]. In essence, the FE arrays are written in terms of fundamental nuclei in CUF, which are invariant of the theory approximation order. Hence, low- (classical) to high-order 1D approximations can be built with ease. In this manner, although 1D, the refined element is able to be tuned to address slender structures as well as more complex problems in which 3D stress states may arise, for example.

Recently, CUF has been extended to deal with linear elastic geometrical nonlinear analyses of beams [24], plates [25] and shells [26]. The results have shown the great capabilities of the FE provided to deal with static large displacement analysis, dynamics [27], and analysis of laminated structures, eventually providing accurate interlaminar stress fields [28]. Extension of CUF-based 1D finite elements to material and geometrical nonlinear analysis of hyperelastic structures is quite promising and is outlined in this paper as follows: (i) first, based on first-invariant hyperelasticity and \bar{F} method, the material Jacobian tensors for various stored energy functions are provided in Section 2; (ii) second, the high order FE model used is briefly discussed in Section 3; (iii) next, Section 4 gives the governing equations and the related FE arrays in unified form; (iv) numerical results are, then, discussed in Section 5; (v) finally, the main conclusions are drawn in Section 6.

2. Nearly incompressible hyperelastic materials

2.1. Strain energy functions

In the case of isotropic hyperelastic materials, the strain energy function Ψ can be expressed in terms of the principal stretches $(\lambda_1, \lambda_2, \lambda_3)$, which are the eigenvalues of the deformation gradient tensor F , or equivalently in terms of the invariants (I_1, I_2, I_3) of the right Cauchy-Green strain tensors $C = F^T F$. It reads:

$$\Psi = \Psi(I_1, I_2, I_3) \quad (1)$$

where

$$\begin{aligned} I_1 &= \text{tr}(C) \\ I_2 &= \frac{1}{2}(I_1^2 - \text{tr}(C^2)) \\ I_3 &= \det(C) \end{aligned} \quad (2)$$

and $\text{tr}(\bullet)$ and $\det(\bullet)$ represent the trace and determinant of a tensor, respectively.

For nearly incompressible materials, the Jacobian determinant (*volume ratio*) $J = \det(F)$ and hence I_3 are approximately equal to unity. According to Flory [29], it is convenient for such a problem to write the gradient tensor as $F = F_{\text{vol}} \bar{F}$, where $F_{\text{vol}} = J^{\frac{1}{3}} \mathbf{1}$ and $\bar{F} = J^{-\frac{1}{3}} F$ represent the volumetric and the isochoric changes, respectively. Reasonably, by setting $C_{\text{vol}} = J^{\frac{2}{3}} \mathbf{1}$ and $\bar{C} = J^{-\frac{2}{3}} C$, we have $C = C_{\text{vol}} \bar{C}$. Now, it is possible to postulate an additive decomposition of the strain energy function and to split Ψ into its volumetric (U) and isochoric ($\bar{\Psi}$) parts as well, to have:

$$\Psi = U(J) + \bar{\Psi}(\bar{I}_1, \bar{I}_2) \quad (3)$$

where \bar{I}_1 and \bar{I}_2 are the first two deviatoric strain invariants, i.e. the invariants of the isochoric right Cauchy-Green tensor \bar{C} .

The volumetric function $U(J)$ acts as a penalization of incompressibility [30]. Several formulations are available in the literature. In this paper we employ the model provided by Sussman and Bathe [7], which states that:

$$U(J) = \frac{1}{D_1} (J - 1)^2 \quad (4)$$

where $D_1 = 2/k$ is the material incompressibility parameter and k is the material bulk modulus.

The literature about the isochoric stored energy potential $\bar{\Psi}$ is vast. Several formulations have been derived over the last decades [31]. Here, we focus on first-invariant hyperelasticity, so that $\bar{\Psi} = \bar{\Psi}(\bar{I}_1)$. Among the others, the neo-Hookean model [32] is quite popular for its simplicity:

$$\bar{\Psi}(\bar{I}_1) = \frac{\mu}{2} (\bar{I}_1 - 3) \quad (5)$$

where μ is the infinitesimal shear modulus. The model of Gent [33], instead, is based on two parameters and it states that:

$$\bar{\Psi}(\bar{I}_1) = -\frac{\mu J_m}{2} \ln\left(1 - \frac{\bar{I}_1 - 3}{J_m}\right) \quad (6)$$

where J_m is the limit value of $(\bar{I}_1 - 3)$. Another formulation investigated in this paper is the Exp-Ln model derived recently by Khajehsaeid *et al.* [34]; it reads:

$$\bar{\Psi}(\bar{I}_1) = A \left[\frac{1}{a} \exp(a(\bar{I}_1 - 3)) + b (\bar{I}_1 - 2) (1 - \ln(\bar{I}_1 - 2)) - \frac{1}{a} - b \right] \quad (7)$$

where $A = \mu/2$ and the parameters b and a adjust moderate and large stretch regimes, respectively. Although the aforementioned strain energy functions have been demonstrated to be effective for polymeric and some biological materials, there are other

formulations that are more appropriate for soft tissue biomechanics, such as the Fung-Demiray model [35]:

$$\bar{\Psi}(\bar{I}_1) = \frac{\beta}{2\alpha} [\exp(\alpha(\bar{I}_1 - 3)) - 1] \quad (8)$$

In Eq. (8) $\beta = \mu$ is the infinitesimal shear modulus and α is the stiffening parameter. Note that in the following derivations other strain energy functions can be used with no loss of generality.

2.2. The material Jacobian tensor

Given the stored-energy function Ψ , the second Piola-Kirchhoff (PK-2) stress tensor can be defined as:

$$\mathbf{S} = 2 \frac{\partial \Psi}{\partial \mathbf{C}} \quad (9)$$

which represents a general form of the constitutive relation. Substituting Eq. (3) into Eq. (9), one can express the PK-2 stress tensor as the sum of a volumetric and an isochoric part.

$$\begin{aligned} \mathbf{S} &= \mathbf{S}^{\text{vol}} + \mathbf{S}^{\text{iso}} \\ \mathbf{S}^{\text{vol}} &= J p \mathbf{C}^{-1} \\ \mathbf{S}^{\text{iso}} &= 2 J^{-\frac{2}{3}} \frac{\partial \bar{\Psi}}{\partial \bar{I}_1} \left(\mathbf{1} - \frac{1}{3} \bar{I}_1 \mathbf{C}^{-1} \right) \end{aligned} \quad (10)$$

where $\mathbf{1}$ is the unity matrix, \mathbf{C}^{-1} is the inverse of the right Cauchy-Green strain tensor and $p = \frac{\partial U}{\partial J}$ is the hydrostatic pressure. The expression of \mathbf{S}^{iso} provided in Eq. (10) holds for first-invariant hyperelasticity models. A more general form of \mathbf{S}^{iso} can be found in the work of Suchocki [36].

According to Holzapfel [37], the nonlinear constitutive equation in Eq. (9) can be transformed into the following incremental form:

$$\Delta \mathbf{S} = \mathcal{C} \cdot \frac{1}{2} \Delta \mathbf{C} \quad (11)$$

which represents a linear relation between the increments of \mathbf{S} and \mathbf{C} . Therefore, Eq. (11) is generally referred to as linearized constitutive equation. Here, \mathcal{C} is the fourth-order elasticity tensor (*material Jacobian tensor*) defined as:

$$\mathcal{C} = \frac{\partial \mathbf{S}}{\partial \mathbf{E}} = 2 \frac{\partial \mathbf{S}}{\partial \mathbf{C}} = 4 \frac{\partial^2 \Psi}{\partial \mathbf{C} \partial \mathbf{C}} \quad (12)$$

where $\mathbf{E} = \frac{1}{2}(\mathbf{C} - \mathbf{1})$ is the Green-Lagrange strain tensor.

Substituting Eq. (10) into Eq. (12) and assuming $U = U(J)$ and $\bar{\Psi} = \bar{\Psi}(\bar{I}_1)$, it is possible to find the following expression of the material Jacobian tensor [38]:

$$\begin{aligned} \mathcal{C} &= \mathcal{C}^{\text{vol}} + \mathcal{C}^{\text{iso}} \\ \mathcal{C}^{\text{vol}} &= J \frac{\partial U}{\partial J} (\mathbf{C}^{-1} \otimes \mathbf{C}^{-1} - 2\mathcal{I}_{\mathbf{C}^{-1}}) + J^2 \frac{\partial^2 U}{\partial J^2} \mathbf{C}^{-1} \otimes \mathbf{C}^{-1} \\ \mathcal{C}^{\text{iso}} &= -\frac{4}{3} J^{-\frac{2}{3}} \frac{\partial \bar{\Psi}}{\partial \bar{I}_1} [\mathbf{1} \otimes \mathbf{C}^{-1} + \mathbf{C}^{-1} \otimes \mathbf{1} \\ &\quad - I_1 (\mathcal{I}_{\mathbf{C}^{-1}} + \frac{1}{3} \mathbf{C}^{-1} \otimes \mathbf{C}^{-1})] + J^{-\frac{4}{3}} \bar{\mathcal{C}}_{\bar{\Psi}} \\ \bar{\mathcal{C}}_{\bar{\Psi}} &= 4 \frac{\partial^2 \bar{\Psi}}{\partial \bar{I}_1^2} [\mathbf{1} \otimes \mathbf{1} - \frac{1}{3} I_1 (\mathbf{1} \otimes \mathbf{C}^{-1} + \mathbf{C}^{-1} \otimes \mathbf{1}) \\ &\quad + \frac{1}{9} I_1^2 \mathbf{C}^{-1} \otimes \mathbf{C}^{-1}] \end{aligned} \quad (13)$$

where \otimes is the dyadic product operator and $\mathcal{I}_{\mathbf{C}^{-1}} = -\partial \mathbf{C}^{-1} / \partial \mathbf{C}$ is the fourth order identity tensor in the reference configuration, see [37].

3. High order finite beam elements

Some recalls about the Carrera Unified Formulation (CUF) and related finite elements (FEs) are provided in this section. Consider a deformed hyperelastic body; the displacement vector $\mathbf{U}(\mathbf{X})$ maps points in the reference configuration $\mathbf{X} = (X, Y, Z)$ to points in the current configuration $\mathbf{x} = (x, y, z)$; i.e. $\mathbf{U} = \mathbf{x} - \mathbf{X}$. Following the standard notation, the deformation gradient can be expressed as:

$$\mathbf{F} = \mathbf{1} + \nabla \mathbf{U} = \mathbf{1} + \mathbf{D} \quad (14)$$

where \mathbf{D} is the displacement gradient. In the domain of CUF, the 3D displacement field of a solid beam with main dimension along the Y -axis, can be expressed as a generic expansion of the *generalized* displacements $U_{\tau}(Y)$:

$$\mathbf{U}(X, Y, Z) = F_{\tau}(X, Z) \mathbf{U}_{\tau}(Y), \quad \tau = 1, 2, \dots, M \quad (15)$$

where F_{τ} represent functions of the coordinates X and Z on the cross-section, M stands for the number of the terms used in the expansion, and the repeated subscript τ indicates summation. The choice of F_{τ} determines the class of the 1D CUF model.

In the case of Taylor Expansion (TE) models, for example, the generalized displacements are expanded around the beam axis by means of a Maclaurin polynomial of truncated order N , see [39]. In other words, F_{τ} functions are polynomials of the type $X^i Z^j$ in the case of TE CUF models. For reasons of completeness, the full 3D displacement field of a quadratic ($N=2$) TE beam model (TE-2) is given in the following:

$$\begin{aligned} U_X(X, Y, Z) &= U_{X_1}(Y) + X U_{X_2}(Y) + Z U_{X_3}(Y) + X^2 U_{X_4}(Y) \\ &\quad + XZ U_{X_5}(Y) + Z^2 U_{X_6}(Y) \\ U_Y(X, Y, Z) &= U_{Y_1}(Y) + X U_{Y_2}(Y) + Z U_{Y_3}(Y) + X^2 U_{Y_4}(Y) \\ &\quad + XZ U_{Y_5}(Y) + Z^2 U_{Y_6}(Y) \\ U_Z(X, Y, Z) &= U_{Z_1}(Y) + X U_{Z_2}(Y) + Z U_{Z_3}(Y) + X^2 U_{Z_4}(Y) \\ &\quad + XZ U_{Z_5}(Y) + Z^2 U_{Z_6}(Y) \end{aligned} \quad (16)$$

Note that TE models are hierarchical and, in the case of a TE model of order N , the number of expansion terms is $M = (N+1)(N+2)/2$. Evidently, the classical beam theories (Euler Bernoulli and Timoshenko theories) are particular cases of the linear CUF TE model (TE-1).

TE CUF-based models have been demonstrated to be very effective for a wide range of applications, see [40, 41]. Nevertheless, they can be inaccurate and thus are not suggested in the case of heterogeneous materials (e.g., laminates) or thin-walled structures [42, 43]. In these cases, Lagrange Expansion (LE) models can be used instead. LE beam theories, in fact, are based on the use of Lagrange-type polynomials to expand the generalized displacements on the beam section domain, F_{τ} . The cross-section physical surface is discretized into a number of expansion sub-

domains, whose polynomial degree depends on the type of Lagrange expansion employed. Three-node linear (LE-3), four-node bilinear (LE-4), nine-node quadratic (LE-9), and sixteen-node cubic (LE-16) beam models have been developed in the framework of CUF. For the sake of brevity, their explicit kinematics is not included here, but they can be found in Carrera and Petrolo [44]. In the following, the 3D displacement field of a quadratic LE-9 beam model is given as an example:

$$\begin{aligned} U_X(X, Y, Z) &= F_1(X, Z) U_{X_1}(Y) + F_2(X, Z) U_{X_2}(Y) \\ &\quad + \dots + F_9(X, Z) U_{X_9}(Y) \\ U_Y(X, Y, Z) &= F_1(X, Z) U_{Y_1}(Y) + F_2(X, Z) U_{Y_2}(Y) \\ &\quad + \dots + F_9(X, Z) U_{Y_9}(Y) \\ U_Z(X, Y, Z) &= F_1(X, Z) U_{Z_1}(Y) + F_2(X, Z) U_{Z_2}(Y) \\ &\quad + \dots + F_9(X, Z) U_{Z_9}(Y) \end{aligned} \quad (17)$$

where F_1, \dots, F_9 form a usual quadratic Lagrange polynomial set. The main feature of LE models is that they make use of local expansions of pure displacement variables, being these arbitrary placed over the cross-section surface. This characteristic enables to capture complex 3D-like solutions at a global/local scale and to increase the accuracy of the solution in particular zones of interest [45].

Independently of the nature of the refined 1D theory adopted, the generalized displacements can be approximated along the beam axis by discretizing the 1D support with finite elements to have:

$$U_\tau(Y) = N_i(Y) U_{\tau i}, \quad i = 1, 2, \dots, N_n \quad (18)$$

In Eq. (18), i stands for summation and the generalized displacements are described as a linear combination of the unknown nodal vector, $U_{\tau i}$, by 1D shape functions, N_i . In the case of classical shape functions, N_n stands for the number of nodes per element and determines the approximation accuracy along the beam axis.

The main advantage of using a compact notation as in Eqs. (15) and (18) is that the governing equations and the FE matrices can be formulated in a unified and hierarchical manner, which is affected neither by the choice of the theory of structure, represented by F_τ , nor by the FE shape functions N_i .

4. Governing equations in unified form

4.1. Internal force vector

According to Pagani and Carrera [24], the Green-Lagrange strain vector can be expressed as follows:

$$\mathbf{E} = \mathbf{E}_l + \mathbf{E}_{nl} = (\mathbf{b}_l + \mathbf{b}_{nl})\mathbf{U} \quad (19)$$

where $\mathbf{U} = \mathbf{U}(X)$ and \mathbf{b}_l and \mathbf{b}_{nl} are the linear and nonlinear differential operators, respectively. They are not given here for the sake of brevity, but they can be found in many reference texts, see for example [46]. Substituting Eqs. (15) and (18) into Eq. (19), one has:

$$\mathbf{E} = (\mathbf{B}_l^{ti} + \mathbf{B}_{nl}^{ti})\mathbf{U}_{\tau i} \quad (20)$$

where \mathbf{B}_l^{ti} and \mathbf{B}_{nl}^{ti} are the two following matrices:

$$\mathbf{B}_l^{ti} = \mathbf{b}_l(F_\tau, N_i) = \begin{bmatrix} F_{\tau, X} N_i & 0 & 0 \\ 0 & F_\tau N_{i, Y} & 0 \\ 0 & 0 & F_{\tau, Z} N_i \\ F_{\tau, Z} N_i & 0 & F_{\tau, X} N_i \\ 0 & F_{\tau, Z} N_i & F_\tau N_{i, Y} \\ F_\tau N_{i, Y} & F_{\tau, X} N_i & 0 \end{bmatrix} \quad (21)$$

and

$$\mathbf{B}_{nl}^{ti} = \frac{1}{2} \begin{bmatrix} U_{X, X} F_{\tau, X} N_i & U_{Y, X} F_{\tau, X} N_i & U_{Z, X} F_{\tau, X} N_i \\ U_{X, Y} F_\tau N_{i, Y} & U_{Y, Y} F_\tau N_{i, Y} & U_{Z, Y} F_\tau N_{i, Y} \\ U_{X, Z} F_{\tau, Z} N_i & U_{Y, Z} F_{\tau, Z} N_i & U_{Z, Z} F_{\tau, Z} N_i \\ U_{X, X} F_{\tau, Z} N_i + U_{X, Z} F_{\tau, X} N_i & U_{Y, X} F_{\tau, Z} N_i + U_{Y, Z} F_{\tau, X} N_i & U_{Z, X} F_{\tau, Z} N_i + U_{Z, Z} F_{\tau, X} N_i \\ U_{X, Y} F_{\tau, Z} N_i + U_{X, Z} F_\tau N_{i, Y} & U_{Y, Y} F_{\tau, Z} N_i + U_{Y, Z} F_\tau N_{i, Y} & U_{Z, Y} F_{\tau, Z} N_i + U_{Z, Z} F_\tau N_{i, Y} \\ U_{X, X} F_\tau N_{i, Y} + U_{X, Y} F_{\tau, X} N_i & U_{Y, X} F_\tau N_{i, Y} + U_{Y, Y} F_{\tau, X} N_i & U_{Z, X} F_\tau N_{i, Y} + U_{Z, Y} F_{\tau, X} N_i \end{bmatrix} \quad (22)$$

In Eqs. (21) and (22), commas denote partial derivatives in the reference configuration.

The governing equations of the problem under consideration are derived from the principle of virtual work, which states that the sum of all the virtual work done by the internal and external forces existing in the system is zero; i.e.

$$\delta W_{\text{int}} - \delta W_{\text{ext}} = 0 \quad (23)$$

where W_{int} is the strain energy, W_{ext} is the work of the external loadings, and δ denotes the variation.

Considering \mathbf{E} and \mathbf{S} in their vectorial form (*Voigt's notation*), the virtual variation of the internal strain energy can be expressed as:

$$\delta W_{\text{int}} = \langle \delta \mathbf{E}^T \mathbf{S} \rangle \quad (24)$$

where $\langle \bullet \rangle = \int_V (\bullet) dX$ is the volume integral in the reference configuration. Now, we can derive the virtual variation of the strain vector from Eq. (20) to have:

$$\delta \mathbf{E} = \delta \left((\mathbf{B}_l^{sj} + \mathbf{B}_{nl}^{sj}) \mathbf{U}_{sj} \right) = (\mathbf{B}_l^{sj} + 2\mathbf{B}_{nl}^{sj}) \delta \mathbf{U}_{sj} \quad (25)$$

Thus,

$$\delta \mathbf{E}^T = \delta \mathbf{U}_{sj}^T (\mathbf{B}_l^{sj} + 2\mathbf{B}_{nl}^{sj})^T \quad (26)$$

In writing Eqs. (25) and (26), the indexes s and j have been respectively used instead of τ and i for the sake of convenience. Substituting Eq. (26) into Eq. (24) gives:

$$\delta W_{\text{int}} = \delta \mathbf{U}_{sj}^T \langle (\mathbf{B}_l^{sj} + 2\mathbf{B}_{nl}^{sj})^T \mathbf{S} \rangle = \delta \mathbf{U}_{sj}^T \mathbf{F}_{\text{int}}^{sj} \quad (27)$$

where \mathbf{S} is found according to Eq. (10) and $\mathbf{F}_{\text{int}}^{sj}$ is the 3×1 fundamental nucleus (FN) of the nonlinear internal force vector. The FN is independent of the theory approximation order and of the choice of the finite element discretizing the beam axis. Once F_τ (i.e. F_s) and N_i (i.e. N_j) are chosen, the FN can be expanded to give the internal force vector of the arbitrarily high order finite beam element; see Carrera *et al.* [23] for further details about the expansion of the FNs.

The FN of the external load vector is not derived here. However, one can reasonably have:

$$\delta W_{\text{ext}} = \delta \mathbf{U}_{sj}^T \mathbf{F}_{\text{ext}}^{sj} \quad (28)$$

Substituting into Eq. (23) and assembling over the final structure, the set of nonlinear algebraic equations can be found:

$$\delta \mathbf{U} : \mathbf{F}_{\text{int}} - \mathbf{F}_{\text{ext}} = 0 \quad (29)$$

4.2. Linearization

Equation (29) constitutes the starting point for finite element calculation of geometrically and physically nonlinear analysis of solids and structures, and it is usually solved through an incremental linearized scheme, typically the Newton-Raphson method. Accordingly, Eq. (29) is written as [47]:

$$\boldsymbol{\varphi}_{\text{res}} \equiv \mathbf{F}_{\text{int}} - \mathbf{F}_{\text{ext}} = 0 \quad (30)$$

where $\boldsymbol{\varphi}_{\text{res}}$ is the vector of the *residual nodal forces*. Equation (30) can now be linearized by expanding $\boldsymbol{\varphi}_{\text{res}}$ in Taylor's series about a known solution, say $(\mathbf{U}, \mathbf{F}_{\text{ext}})$. Omitting the second-order terms, one has

$$\begin{aligned} \boldsymbol{\varphi}_{\text{res}}(\mathbf{U} + \delta \mathbf{U}, \mathbf{F}_{\text{ext}} + \delta \mathbf{F}_{\text{ext}}) &= \boldsymbol{\varphi}_{\text{res}}(\mathbf{U}, \mathbf{F}_{\text{ext}}) + \frac{\partial \boldsymbol{\varphi}_{\text{res}}}{\partial \mathbf{U}} \delta \mathbf{U} \\ &+ \frac{\partial \boldsymbol{\varphi}_{\text{res}}}{\partial \mathbf{F}_{\text{ext}}} \delta \lambda \hat{\mathbf{F}}_{\text{ext}} = 0 \end{aligned} \quad (31)$$

where $\frac{\partial \boldsymbol{\varphi}_{\text{res}}}{\partial \mathbf{U}} = \mathbf{K}_T$ is the *tangent stiffness matrix*, and $\frac{\partial \boldsymbol{\varphi}_{\text{res}}}{\partial \mathbf{F}_{\text{ext}}} = -\mathbf{1}$. In Eq. (31) it was assumed that the load varies directly with the vector of the reference loadings $\hat{\mathbf{F}}_{\text{ext}}$ and has a rate of change equal to the load parameter λ , i.e. $\mathbf{F}_{\text{ext}} = \lambda \hat{\mathbf{F}}_{\text{ext}}$. Equation (31) is written in a more compact form as follows:

$$\mathbf{K}_T \delta \mathbf{U} = \delta \lambda \hat{\mathbf{F}}_{\text{ext}} - \boldsymbol{\varphi}_{\text{res}} \quad (32)$$

Since the load-scaling parameter λ is taken as a variable, an additional governing equation is required and this is given by a constraint relationship $c(\delta \mathbf{U}, \delta \lambda)$ to finally give:

$$\begin{cases} \mathbf{K}_T \delta \mathbf{U} = \delta \lambda \hat{\mathbf{F}}_{\text{ext}} - \boldsymbol{\varphi}_{\text{res}} \\ c(\delta \mathbf{U}, \delta \lambda) = 0 \end{cases} \quad (33)$$

Depending on the constraint equation, different incremental schemes can be implemented. In this paper, a path-following method is employed in which the constraint equation is a function of both displacement and load parameter variations. In particular, we employ an arc-length strategy as proposed by Criefield [48, 49]; hence the constraint relationship corresponds to a multi-dimensional sphere. Furthermore, to avoid *doubling back* on the original load-deflection path for the given iteration step, the solution of the *consistent-linearized* constraint equation is used as proposed by Carrera [50] to advance in the calculation. Details about the solution scheme implemented are not given here although. Interested readers are referred to Ref. [24].

4.3. Tangent stiffness matrix

Assuming that the loading is conservative so that the linearization of the virtual variation of the external loads is null, i.e. $\delta^2 W_{\text{ext}} = 0$, the analytical expression of the tangent matrix can be obtained from linearizing the virtual variation of the strain energy as follows:

$$\begin{aligned} \delta^2 W_{\text{int}} &= \langle \delta(\delta \mathbf{E}^T \mathbf{S}) \rangle \\ &= \langle \delta \mathbf{E}^T \delta \mathbf{S} \rangle + \langle \delta(\delta \mathbf{E}^T) \mathbf{S} \rangle \\ &= \delta \mathbf{U}_{sj}^T (\mathbf{K}_0^{ij\tau s} + \mathbf{K}_{T_1}^{ij\tau s} + \mathbf{K}_{\sigma}^{ij\tau s}) \delta \mathbf{U}_{\tau i} \\ &= \delta \mathbf{U}_{sj}^T \mathbf{K}_T^{ij\tau s} \delta \mathbf{U}_{\tau i} \end{aligned} \quad (34)$$

Each nonlinear contribution in the right-hand-side of Eq. (34)₂ is now considered separately.

The first term, $\langle \delta \mathbf{E}^T \delta \mathbf{S} \rangle$, demands for the linearized constitutive relation provided in Eqs. (11) and (12); it reads:

$$\delta \mathbf{S} = \mathcal{C} \delta \mathbf{E} = \mathcal{C} (\mathbf{B}_l^{\tau i} + 2 \mathbf{B}_{nl}^{\tau i}) \delta \mathbf{U}_{\tau i} \quad (35)$$

Hence, considering Eqs. (26) and (35) gives:

$$\begin{aligned} \langle \delta \mathbf{E}^T \delta \mathbf{S} \rangle &= \delta \mathbf{U}_{sj}^T \langle (\mathbf{B}_l^{sj} + 2 \mathbf{B}_{nl}^{sj})^T \mathcal{C} (\mathbf{B}_l^{\tau i} + 2 \mathbf{B}_{nl}^{\tau i}) \rangle \delta \mathbf{U}_{\tau i} \\ &= \delta \mathbf{U}_{sj}^T \mathbf{K}_0^{ij\tau s} \delta \mathbf{U}_{\tau i} + \delta \mathbf{U}_{sj}^T (2 \mathbf{K}_{lnl}^{ij\tau s}) \delta \mathbf{U}_{\tau i} \\ &+ \delta \mathbf{U}_{sj}^T \mathbf{K}_{nll}^{ij\tau s} \delta \mathbf{U}_{\tau i} + \delta \mathbf{U}_{sj}^T (2 \mathbf{K}_{nlnl}^{ij\tau s}) \delta \mathbf{U}_{\tau i} \\ &= \delta \mathbf{U}_{sj}^T (\mathbf{K}_0^{ij\tau s} + \mathbf{K}_{T_1}^{ij\tau s}) \delta \mathbf{U}_{\tau i} \end{aligned} \quad (36)$$

where

$$\begin{aligned} \mathbf{K}_0^{ij\tau s} &= \langle (\mathbf{B}_l^{sj})^T \mathcal{C} \mathbf{B}_l^{\tau i} \rangle & \mathbf{K}_{lnl}^{ij\tau s} &= \langle (\mathbf{B}_l^{sj})^T \mathcal{C} \mathbf{B}_{nl}^{\tau i} \rangle \\ \mathbf{K}_{nll}^{ij\tau s} &= 2 \langle (\mathbf{B}_{nl}^{sj})^T \mathcal{C} \mathbf{B}_l^{\tau i} \rangle & \mathbf{K}_{nlnl}^{ij\tau s} &= 2 \langle (\mathbf{B}_{nl}^{sj})^T \mathcal{C} \mathbf{B}_{nl}^{\tau i} \rangle \end{aligned} \quad (37)$$

and $\mathbf{K}_{T_1}^{ij\tau s} = 2 \mathbf{K}_{lnl}^{ij\tau s} + \mathbf{K}_{nll}^{ij\tau s} + 2 \mathbf{K}_{nlnl}^{ij\tau s}$ is the sum of order-one and order-two nonlinear matrices. As in the case of the internal force vector, the matrices $\mathbf{K}_0^{ij\tau s}$, $\mathbf{K}_{lnl}^{ij\tau s}$, $\mathbf{K}_{nll}^{ij\tau s}$, and $\mathbf{K}_{nlnl}^{ij\tau s}$ are given in terms of FNs. These are 3×3 matrices that, given the cross-sectional functions ($F_{\tau} = F_s$, for $\tau = s$) and the shape functions ($N_i = N_j$, for $i = j$), can be expanded by using the indexes $\tau, s = 1, \dots, M$ and $i, j = 1, \dots, N_n$ in order to obtain the elemental secant stiffness matrix of any arbitrarily refined beam model. In other words, by opportunely choosing the beam kinematics (i.e., by choosing F_{τ} as well as the number of expansion terms M) classical to higher-order beam theories and related stiffness arrays can be implemented in an automatic manner by exploiting the index notation of CUF.

The evaluation of the contribution $\langle \delta(\delta \mathbf{E}^T) \mathbf{S} \rangle$ in Eq. (34) requires the linearization of the nonlinear geometrical relations [24]:

$$\delta(\delta \mathbf{E}^T) = \left\{ \begin{array}{l} \delta U_{X_{\tau i}} \delta U_{X_{s j}} \\ \delta U_{Y_{\tau i}} \delta U_{Y_{s j}} \\ \delta U_{Z_{\tau i}} \delta U_{Z_{s j}} \end{array} \right\}^T (\mathbf{B}_{nl}^*)^T \quad (38)$$

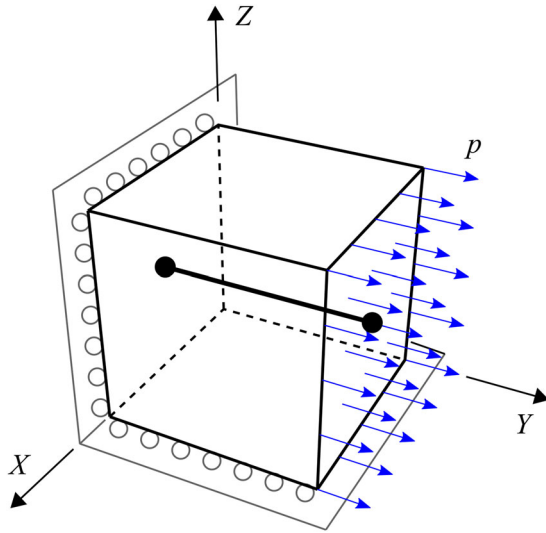


Figure 1. Geometry and boundary conditions used for uniaxial tension test.

where

$$\mathbf{B}_{nl}^* = \begin{bmatrix} F_{\tau,x}F_{s,x}N_iN_j & F_{\tau,x}F_{s,x}N_iN_j & F_{\tau,x}F_{s,x}N_iN_j \\ F_{\tau,z}F_{s,x}N_iN_j & F_{\tau,z}F_{s,x}N_iN_j & F_{\tau,z}F_{s,x}N_iN_j \\ F_{\tau,z}F_{s,z}N_iN_j & F_{\tau,z}F_{s,z}N_iN_j & F_{\tau,z}F_{s,z}N_iN_j \\ F_{\tau,x}F_{s,z}N_iN_j + F_{\tau,z}F_{s,x}N_iN_j & F_{\tau,x}F_{s,z}N_iN_j + F_{\tau,z}F_{s,x}N_iN_j & F_{\tau,x}F_{s,z}N_iN_j + F_{\tau,z}F_{s,x}N_iN_j \\ F_{\tau,z}F_{s,x}N_iN_j + F_{\tau,x}F_{s,z}N_iN_j & F_{\tau,z}F_{s,x}N_iN_j + F_{\tau,x}F_{s,z}N_iN_j & F_{\tau,z}F_{s,x}N_iN_j + F_{\tau,x}F_{s,z}N_iN_j \\ F_{\tau,x}F_{s,x}N_iN_j + F_{\tau,z}F_{s,x}N_iN_j & F_{\tau,x}F_{s,x}N_iN_j + F_{\tau,z}F_{s,x}N_iN_j & F_{\tau,x}F_{s,x}N_iN_j + F_{\tau,z}F_{s,x}N_iN_j \end{bmatrix} \quad (39)$$

Given Eq. (38) and after simple manipulations, the following passages are fairly clear:

$$\begin{aligned} \langle \delta(\delta E^T) \mathbf{S} \rangle &= \left\langle \begin{Bmatrix} \delta U_{X_{\tau i}} \delta U_{X_{s j}} \\ \delta U_{Y_{\tau i}} \delta U_{Y_{s j}} \\ \delta U_{Z_{\tau i}} \delta U_{Z_{s j}} \end{Bmatrix}^T (\mathbf{B}_{nl}^*)^T \mathbf{S} \right\rangle \\ &= \delta \mathbf{U}_{s j}^T \langle \text{diag}((\mathbf{B}_{nl}^*)^T \mathbf{S}) \rangle \delta \mathbf{U}_{\tau i} \\ &= \delta \mathbf{U}_{s j}^T \mathbf{K}_{\sigma}^{ijrs} \delta \mathbf{U}_{\tau i} \end{aligned} \quad (40)$$

where $\text{diag}((\mathbf{B}_{nl}^*)^T \mathbf{S})$ is the 3×3 diagonal matrix, whose diagonal terms are the components of the vector $(\mathbf{B}_{nl}^*)^T \mathbf{S}$. The term elaborated in Eq. (40) defines a tangent term arising from the nonlinear form of the strain-displacement equations and is often called the geometric stiffness [51], of which $\mathbf{K}_{\sigma}^{ijrs}$ is the fundamental nucleus.

5. Numerical results

5.1. Uniaxial tension

The first problem deals with uniaxial tension, for which the analytical solution is easy to determine. In this case, considering first-invariant hyperelastic materials, we have:

$$\bar{I}_1 = I_1 = \lambda_1^2 + \frac{2}{\lambda_1} \quad \bar{\Psi} = \Psi(\lambda_1) \quad (41)$$

where λ_1 is the stretch ratio in the traction direction, eigenvalue of \mathbf{F} . Note that in Eq. (41) the volume ratio J is assumed equal to unity. Now, according to Holzapfel [37]:

Table 1. Material parameters used for the uniaxial tension test.

Model	Parameters	UM
Neo-Hookean [32]	$\mu = 0.27$	MPa
Gent [33]	$\mu = 0.27$	MPa
	$J_m = 85.91$	-
Exp-Ln [34]	$A = 0.195$	MPa
	$a = 0.018$	-
	$b = 0.22$	-
Fung-Demiray [35]	$\beta = 0.2$	MPa
	$\alpha = 16$	-

The penalty parameter D_1 is equal to $33 \times 10^{-9} \text{ MPa}^{-1}$ for all the cases.

$$P_{11} = \frac{\partial \Psi}{\partial \lambda_1} = \frac{\partial \Psi}{\partial I_1} \frac{\partial I_1}{\partial \lambda_1} = 2 \frac{\partial \Psi}{\partial I_1} \left(\lambda_1 - \frac{1}{\lambda_1} \right) \quad (42)$$

where P_{11} is the Lagrangian stress, i.e. the first Piola-Kirchhoff (PK-1) stress component, and $\frac{\partial \Psi}{\partial I_1}$ can be derived from Eqs. (5), (6) and similar. Given P_{11} , the PK-2 (S_{11}) and the Cauchy (σ_{11}) stress components can be found straightforwardly:

$$S_{11} = \frac{1}{\lambda_1} \frac{\partial \Psi}{\partial \lambda_1} = \frac{1}{\lambda_1} P_{11} \quad (43)$$

$$\sigma_{11} = J^{-1} \lambda_1 \frac{\partial \Psi}{\partial \lambda_1} = \lambda_1 P_{11} \quad (44)$$

For verification purpose, the aforementioned exact solution is compared to numerical solutions obtained with the present CUF-based finite element. We consider a cubic sample, whose geometry and boundary conditions are depicted in Figure 1. The cubic sample is modeled as a beam, discretized with one single finite element along the Y-axis. For this particular case, a linear (two-node, B2) Lagrangian beam element is utilized. On the other hand, the theory of structure, i.e. the beam cross-section approximation, is bilinear in XZ. In other words, one L4 approximation polynomial is used as F_{τ} ; see Eq. (15) and Ref. [44].

All the strain energy functions described in Eqs. (5)–(8) are considered in the analysis and the material parameters employed are given in Table 1. The stress-stretch curves are given in Figure 2. Also, deformed states of the cubic samples under tension made of Gent-type material are shown in Figure 3. The comparison demonstrates a perfect matching between the proposed finite element model and the analytical solutions, for both small to large strain regimes. Although not documented here for the sake of brevity, the same analysis has been performed also by considering a larger number of finite elements and different F_{τ} approximation functions (both TE and higher-order LE). For all the cases, the analytical solutions were perfectly superimposed to CUF-based simulation results.

5.2. Neo-Hookean beam subjected to bending

In the second analysis case, a hyperelastic clamped-free beam subjected to a tip transverse force is considered. The beam has a solid rectangular cross-section (100 mm thick \times 150 mm height), whereas the length to thickness ratio is equal to 100. The transverse loading is $F_0 = 269.5 \text{ N}$. The structure is made of soft material (here modeled with the neo-Hookean strain energy function) with infinitesimal

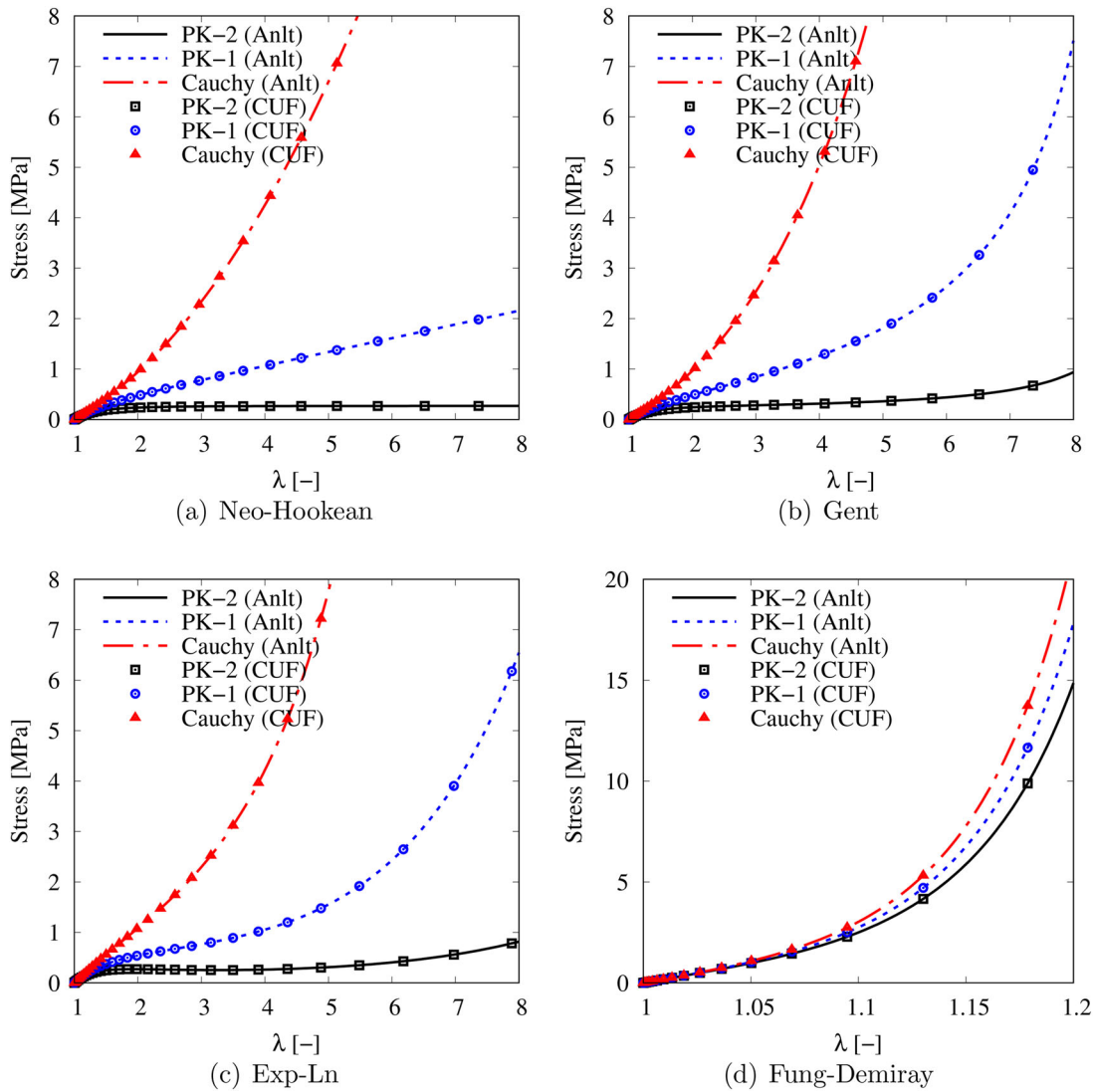


Figure 2. Uniaxial tension for various hyperelastic models; comparison of analytical and CUF-based FE results.

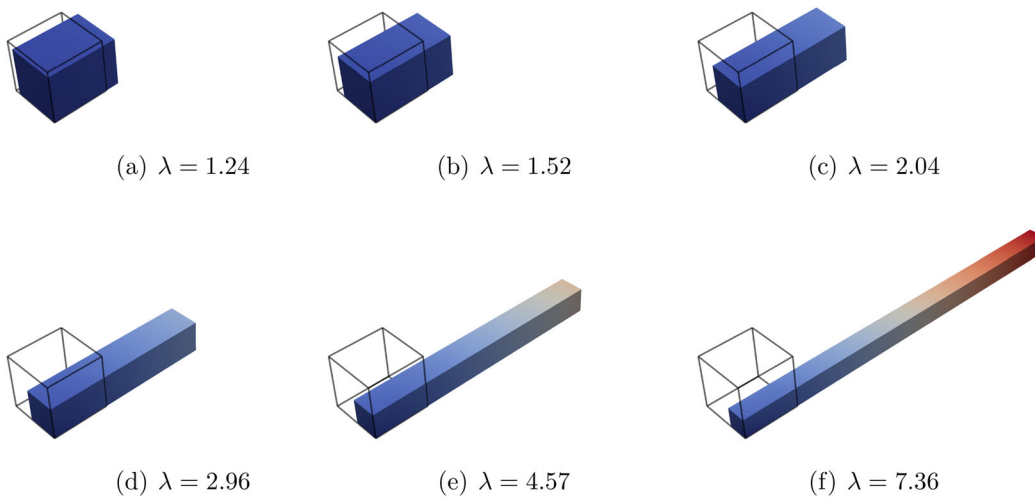


Figure 3. Deformed states of the cube subjected to uniaxial tension and made of hyperelastic Gent-type material. 1B2-1L4 CUF-based finite element model.

shear modulus $\mu = 50$ MPa and bulk modulus $k = 2\mu/3$. The same problem is addressed by Maas *et al.* [52], who provide also an analytical solution and some finite element results.

The problem under consideration is depicted in Figure 4. The figure shows the geometry, the boundary conditions and some deformed states of the beam subjected to large deformations. The results demonstrated in this pictures are

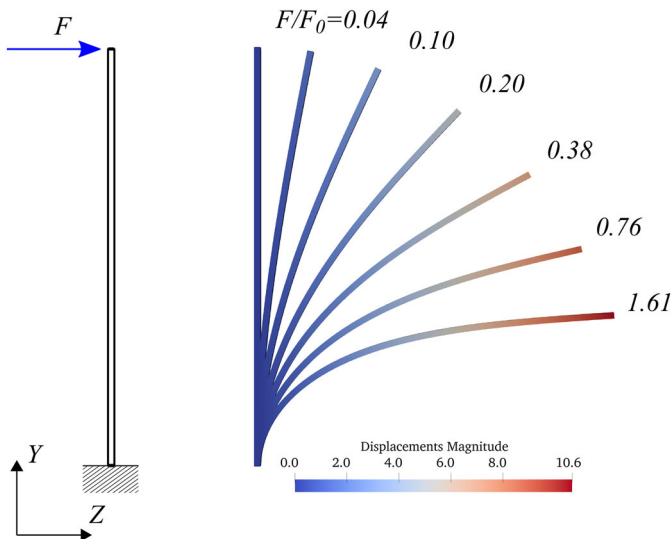


Figure 4. Neo-Hookean cantilever. Geometry, boundary conditions and deformed states for various load levels. $F_0 = 269.35$ N.

obtained by the present high-order CUF beam model. A more detailed study of the equilibrium state of the cantilever is shown in Figure 5. In performing the analyses reported, four-node cubic shape functions (B4) have been used to discretize the beam axis. The convergence analysis of Figure 5a shows that five elements are enough for providing accurate results. Figure 5b, on the other hand, shows the effect of different beam theories (both TE and LE). It is demonstrated that low- and high-order beam models provide all good results in terms of displacement prediction. This is quite reasonable because the beam is very slender.

Different beam theories are also compared in Figure 6, which gives the through-the-thickness distribution on the midspan cross-section of the PK-2 axial and transverse shear stress components for a large loading. This figure highlights the importance of high-order kinematics in the case of stress prediction. Indeed, although low-order beam theories provide good accuracy in terms of S_{YY} , at least a third-order

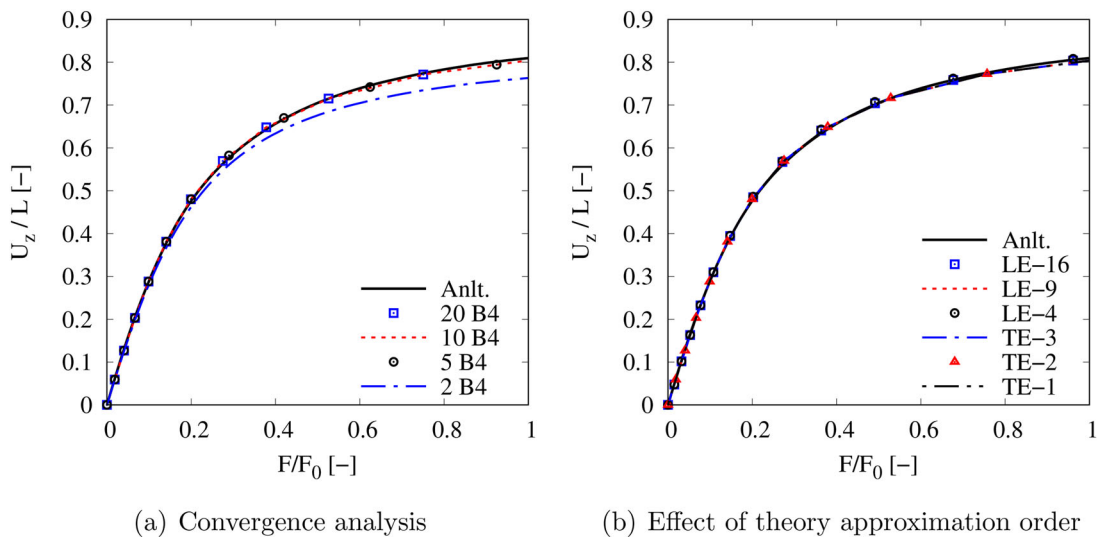


Figure 5. Equilibrium curves (tip displacement vs. loading) of the neo-Hookean beam subjected to bending.

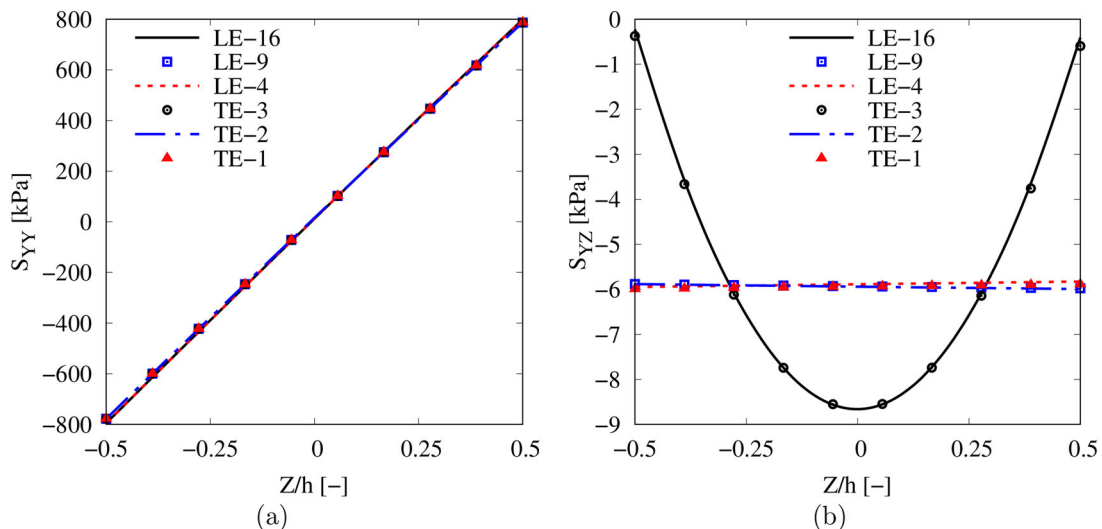


Figure 6. Effect of the theory approximation order on the through-the-thickness distribution of PK-2 axial and transverse shear stress components on the midspan cross-section of the neo-Hookean beam subjected to a transverse loading $F/F_0 = 1.05$.

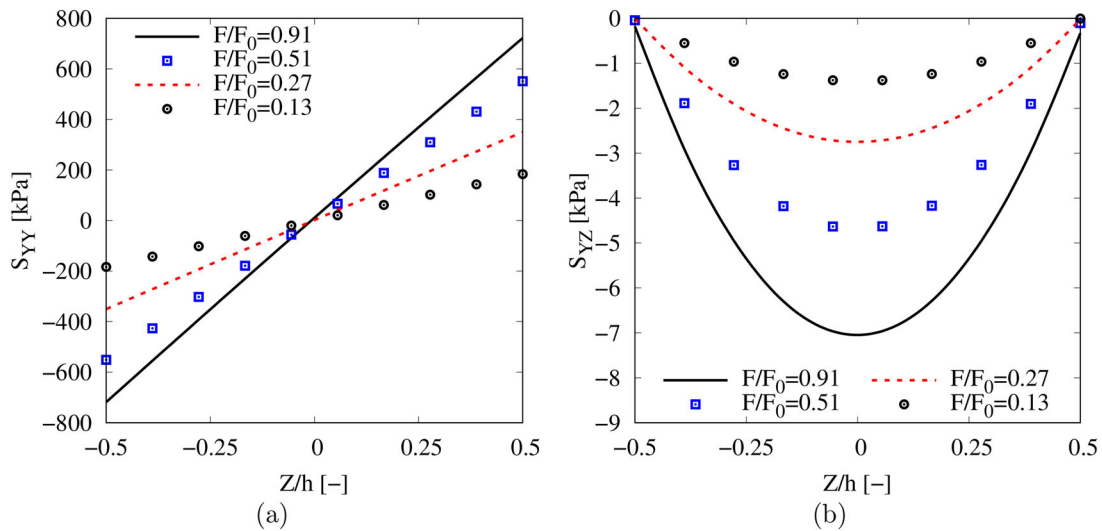


Figure 7. Through-the-thickness distribution of PK-2 axial and transverse shear stress components on the midspan cross-section of the neo-Hookean beam for various transverse loadings. LE-16 CUF finite element beam model.

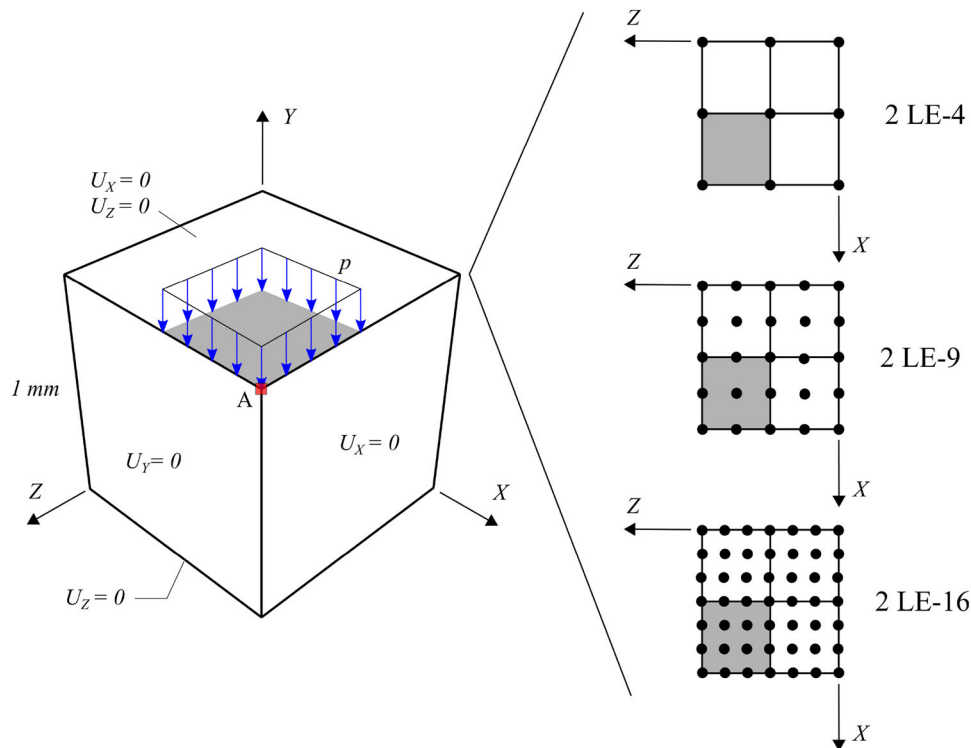


Figure 8. Incompressible block under pressure: geometry, boundary conditions and cross-section models adopted.

beam model (e.g. TE-3 and LE-16) is required to correctly predict the shear stresses S_{YZ} . As a final result for the cantilever hyperelastic beam, Figure 7 shows the PK-2 stress state for various load levels. These latest results derive from a CUF-based finite beam model discretized with 10 B4 and making use of a LE-16 approximation over the cross-section.

5.3. Nearly incompressible block under compression

In this section, the nearly incompressible block under pressure, introduced by Reese *et al.* [53] and later considered by many authors (see for example [9, 30, 54, 55]), is studied.

The problem under consideration is depicted in Figure 8. It consists of a cube loaded by an applied pressure in the center of the top face. Note that only a quarter of the cube is modeled with each side equal to 1 mm. Symmetric Dirichlet boundary conditions are applied to the vertical faces and the top face is fixed in the horizontal plane. The cube is made of neo-Hookean material with $\mu = 80.194$ MPa and $k = 400'953.269$ MPa.

In the framework of the present paper, the block is modeled via refined 1D finite elements laying along the Y-axis. In contrast, LE expansions are used in the cross-section domain (TE exhibits poor convergence for this problem and are not reported hereafter). The models are referred to as N

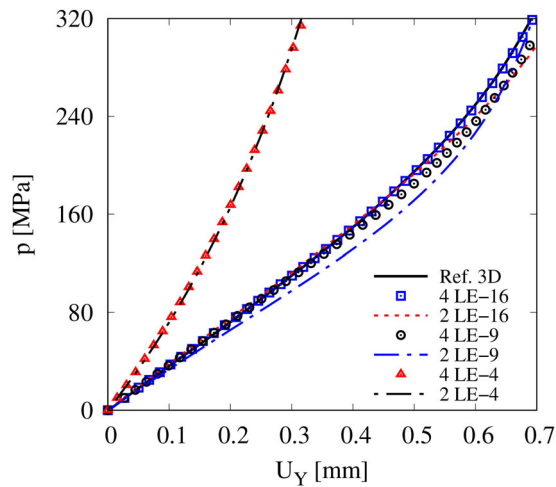


Figure 9. Equilibrium curves (vertical displacement at point A vs. applied pressure) of the block under compression. Comparison between various CUF-based FE models and reference solution from Caylak and Mahnken [9].

Table 2. Vertical displacement U_Y [mm] at point A for various 1 D CUF models of the block under compression for various pressure levels and comparison with results from the literature.

Model	$p = 320$ MPa	$p = 640$ MPa	dof's
Caylak and Mahnken [9]	0.6935	–	(202'463 tet. el.)
Karavelas <i>et al.</i> [30]	0.6979	0.8527	$10^5 +$
4 LE-16	0.6925	0.8504	6591
2 LE-16	0.7383	0.9306	1029
4 LE-9	0.7149	0.8583	2187
2 LE-9	0.6952	0.8014	375
4 LE-4	0.3266	0.4684	375
2 LE-4	0.3183	0.4591	81

LE-4, N LE-9 or N LE-16, where N is the number of elements adopted along X , Y and Z (see Figure 8). For consistency reason, linear (B2), quadratic (B3) and cubic (B4) shape functions are employed to discretize the longitudinal axis in the case, respectively, of LE-4, LE-9 and LE-16 beam models. Furthermore, a reduced order integration is utilized to calculate the integrals of the shape functions $\int N_i N_j$ to attenuate locking phenomena.

Figure 9 shows the vertical displacement U_Y of point A (center of the block) as a function of the applied pressure p for various LE beam models and a reference solution based on a stabilized mixed U - p three-dimensional finite element formulation [9]. The equilibrium curves range from $p = 0$ to $p = 320$ MPa; higher values are not given in the reference solution. It is clear that the LE-4 models are affected by the locking. In contrast, quadratic (LE-9) as well as cubic (LE-16) beam formulations provides good results. In particular, the 4 LE-16 model matches perfectly the 3D reference solution.

A further assessment is provided in Table 2, where the proposed model is compared to 3D finite elements for both moderate ($p = 320$ MPa) and large ($p = 640$ MPa) pressure loads. In detail, the refined LE models are here compared with the best solution from Caylak and Mahnken [9], based on a 3D model using more than 200,000 tetrahedral mixed solid elements, and with a pressure-projection stabilized finite element model from Karavelas *et al.* [30]. For the latter, the results were extrapolated from a plot and, from the

many solutions provided in the paper, the first model giving convergent solution for both the pressure levels was selected.

As a final result, Figure 10 shows some deformed state of the solid block subjected to different pressure loads. The deformations depicted were calculated by using the present LE-16 beam model. The 3D mesh shown in the figure is a plotting mesh used for convenience. The mathematical model is 1D indeed.

5.4. Thick hyperelastic cylinder

The thick hyperelastic cylindrical structure shown in Figure 11 is considered as the last analysis case. For symmetry reason, only one-quarter of the structure is considered as in [56]. The inner radius is equal to 8 cm, whereas the thickness is $t = 2$ cm. The length of the cylindrical portion analyzed is equal to $L = 15$ cm. A neo-Hookean material model is adopted with infinitesimal shear modulus $\mu = 6000$ kN/cm² and bulk modulus $k = 280,000$ kN/cm². Note that in this case the Poisson ratio is $\nu = 0.4$, hence no volumetric locking is expected.

This problem was already analyzed in the literature by many authors using shell or brick elements [53, 54, 56]. Our objective here is to demonstrate the proposed beam model can deal with large cross-sectional deformation, thus can be used effectively for soft thin-walled structures. Indeed, the cylinder is modeled by using one single four-node cubic finite element (B4) along the beam axis laying on Y . On the other hand, LE-16 approximations are employed on the beam cross-section because of their superior convergence capabilities demonstrated in the previous sections.

The analyses conducted show that one B4 beam element is enough to guarantee convergence. In contrast, the cross-section needs to be discretized using a number of LE-16 sub-domains. Table 3 gives the transverse displacement at point A for various LE-16 models and $p = 999.47$ kN/cm. They are referred to as N LE-16, where N is the number of elements employed along the circumferential direction. One single element along the thickness was instead enough to catch the bending effects. The table also shows the difference between the proposed approach and some results from the literature, even in terms of number of degrees of freedom.

Analogous comparison with references is also possible from Figure 12, which presents the equilibrium curves resulting from the proposed 1D formulation. Here, the convergence of the models employed can be appreciated. Note that Büchter *et al.* [56] used a 7-parameter nonlinear shell formulation based on the enhanced assumed strain concept. The same problem was solved by Reese *et al.* [53] with a locking-free brick element using reduced integration plus stabilization concept. Finally, Elguedj *et al.* [54] performed detailed analysis of the same structure with NURBS-based isogeometric solutions and \bar{F} method.

For completeness, Figure 13 shows some important deformed states of the cylindrical beam under different line load levels, from $p = 179$ kN/cm to $p = 886$ kN/cm. As in the previous cases, note that the one shown in the figures is

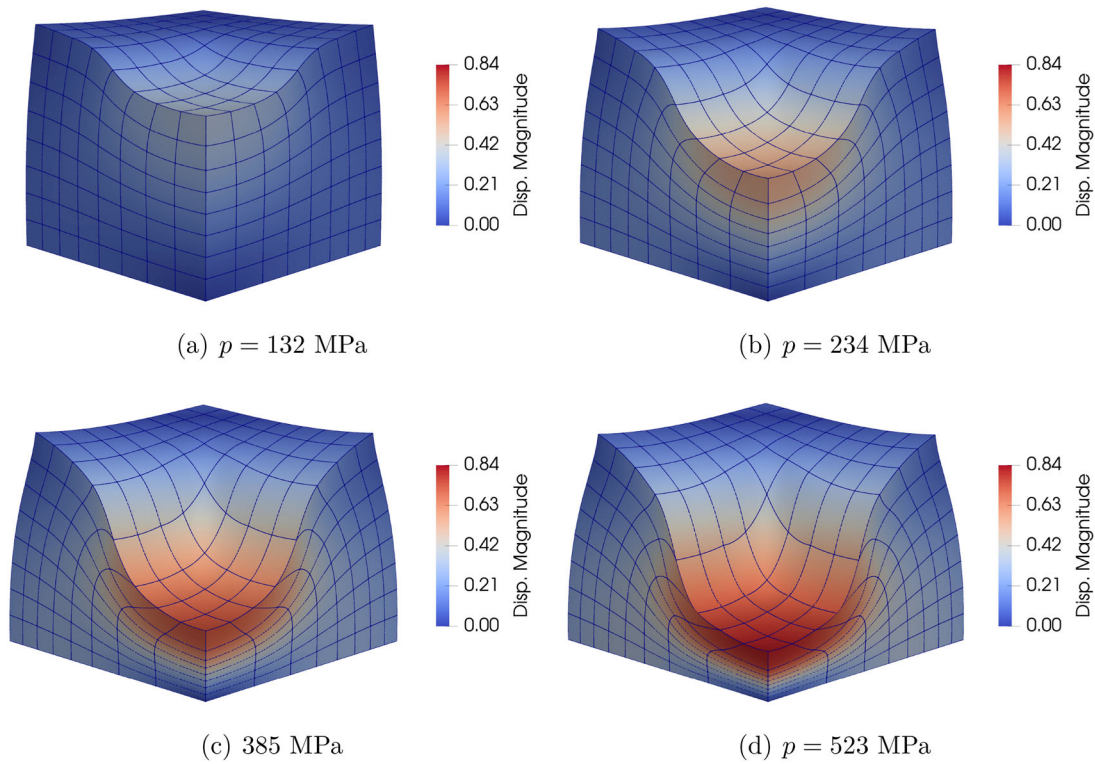


Figure 10. Deformed states of the nearly incompressible block under compression according to the 4 LE-16 CUF beam model. Displacement magnitude in mm.

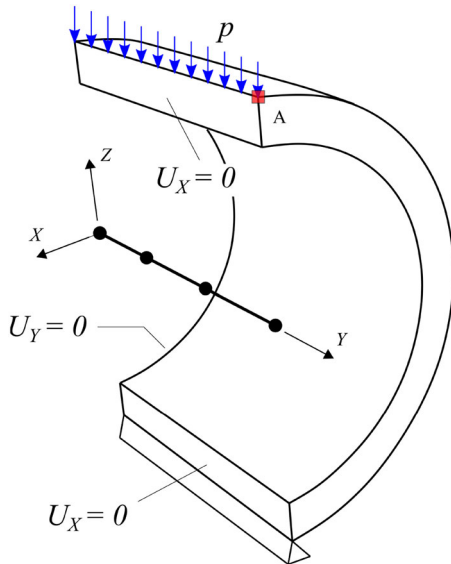


Figure 11. Geometry, boundary conditions and FE discretization of the thick cylinder.

Table 3. Transverse displacement at point A for $p = 999.47$ kN/cm and dof's.

Model	U_z [cm]	dof's
Büchter <i>et al.</i> [56]	16.00	3003
Reese <i>et al.</i> [53]	16.49	4902
Elguedj <i>et al.</i> [54]	16.94	-
16 LE-16	16.88	2352
8 LE-16	16.77	1200
4 LE-16	15.85	624

Comparison between CUF 1D FE models the pinched hyperelastic thick cylinder and solutions from the literature.

only a mesh used for plotting convenience and is representative neither of the actual mathematical model nor of the discretization used for the analysis.

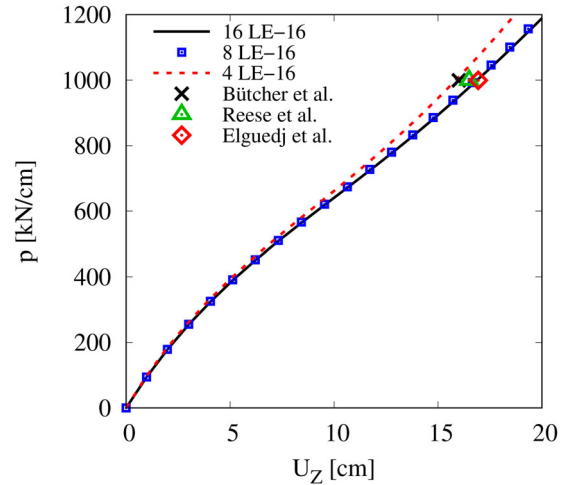


Figure 12. Equilibrium curves (vertical displacement at point A vs. distributed line load) of the thick cylinder. Comparison between LE-16 models and reference solutions from Büchter *et al.* [56], Reese *et al.* [53], and Elguedj *et al.* [54].

6. Conclusions

This paper has discussed one-dimensional (1D) high order finite elements for the analysis of first-invariant hyperelastic materials and structures. The model is based on the Carrera Unified Formulation (CUF), according to which classical to refined beam theories can degenerate into an arbitrary, recursive approximation of the generalized 1D unknowns. The governing equations and the related FE arrays are given accordingly by using a few fundamental nuclei, which are invariant of the theory approximation order.

Several problems are considered and the effect of the theory approximation order on the convergence and the

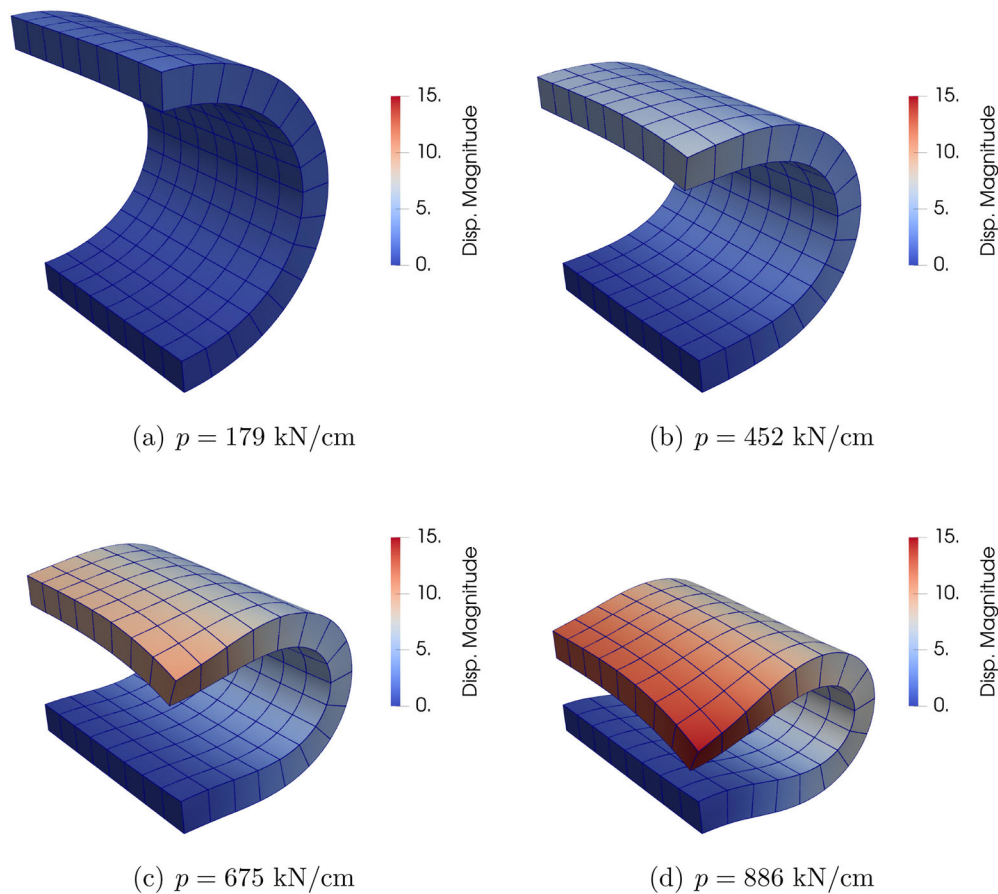


Figure 13. Deformed states of the hyperelastic thick cylinder according to the 8 LE-16 CUF beam model. Displacement magnitude in cm.

accuracy of the solutions is studied in detail. The numerical investigation has demonstrated that the model provided is able to deal effectively with the analysis of soft materials and structures, from moderate to deep nonlinear regimes. Future works will deal with the extension to plates and shells and to inhomogeneous, eventually anisotropic, soft structures.

Funding

This work is part of a project that has received funding from the European Research Council (ERC) under the European Union's Horizon 2020 research and innovation programme (Grant agreement No. 850437).

Data availability

The data that support the findings of this study are available from the corresponding author, AP, upon reasonable request.

References

- [1] A. Leber, et al., Compressible and electrically conducting fibers for large-area sensing of pressures, *Adv. Funct. Mater.*, vol. 30, no. 1, pp. 1904274, 2020. DOI: [10.1002/adfm.201904274](https://doi.org/10.1002/adfm.201904274).
- [2] F. López Jiménez, P. Upadhyaya, J. Liljenhjerter, P. M. Reis, and S. Kumar, Soft optical composites for tunable transmittance, *Extreme Mech. Lett.*, vol. 9, pp. 297–303, 2016. DOI: [10.1016/j.eml.2016.09.003](https://doi.org/10.1016/j.eml.2016.09.003).
- [3] Y. Cao, J. Zhu, B. Wu, and W. Chen, Axisymmetric free vibration of soft electroactive circular plates under biasing fields, *Acta Mech. Solida Sin.*, vol. 34, no. 3, pp. 326–345, 2021. DOI: [10.1007/s10338-020-00211-x](https://doi.org/10.1007/s10338-020-00211-x).
- [4] R. W. Penn, Volume changes accompanying the extension of rubber, *Trans. Soc. Rheol.*, vol. 14, no. 4, pp. 509–517, 1970. DOI: [10.1122/1.549176](https://doi.org/10.1122/1.549176).
- [5] I. Babuška, and M. Suri, Locking effects in the finite element approximation of elasticity problems, *Numer. Math.*, vol. 62, no. 1, pp. 439–463, 1992. DOI: [10.1007/BF01396238](https://doi.org/10.1007/BF01396238).
- [6] T. J. R. Hughes, and D. S. Malkus, A general penalty/mixed equivalence theorem for anisotropic, incompressible finite elements. In S. N. Atluri, R. H. Gallagher, and O. C. Zienkiewicz (ed.), *Hybrid and Mixed Finite Element Methods*. Wiley, New York, USA, 1983.
- [7] T. Sussman, and K.-J. Bathe, A finite element formulation for nonlinear incompressible elastic and inelastic analysis, *Comput. Struct.*, vol. 26, no. 1-2, pp. 357–409, 1987. DOI: [10.1016/0045-7949\(87\)90265-3](https://doi.org/10.1016/0045-7949(87)90265-3).
- [8] J. C. Simo, and F. Armero, Geometrically non-linear enhanced strain mixed methods and the method of incompatible modes, *Int. J. Numer. Meth. Eng.*, vol. 33, no. 7, pp. 1413–1449, 1992. DOI: [10.1002/nme.1620330705](https://doi.org/10.1002/nme.1620330705).
- [9] I. Caylak, and R. Mahnken, Stabilization of mixed tetrahedral elements at large deformations, *Int. J. Numer. Meth. Eng.*, vol. 90, no. 2, pp. 218–242, 2012. DOI: [10.1002/nme.3320](https://doi.org/10.1002/nme.3320).
- [10] A. Düster, S. Hartmann, and E. Rank, p-FEM applied to finite isotropic hyperelastic bodies, *Comput. Methods Appl. Mech. Eng.*, vol. 192, no. 47-48, pp. 5147–5166, 2003. DOI: [10.1016/j.cma.2003.07.003](https://doi.org/10.1016/j.cma.2003.07.003).
- [11] J. C. Simo, R. L. Taylor, and K. S. Pister, Variational and projection methods for the volume constraint in finite deformation

- elasto-plasticity, *Comput. Methods Appl. Mech. Eng.*, vol. 51, no. 1-3, pp. 177–208, 1985. DOI: [10.1016/0045-7825\(85\)90033-7](https://doi.org/10.1016/0045-7825(85)90033-7).
- [12] S. S. Antman, and F. Schuricht, Incompressibility in rod and shell theories, *Esaim: M2an.*, vol. 33, no. 2, pp. 289–304, 1999. DOI: [10.1051/m2an:1999116](https://doi.org/10.1051/m2an:1999116).
- [13] M. M. Attard, Finite strain-beam theory, *Int. J. Solids Struct.*, vol. 40, no. 17, pp. 4563–4584, 2003. DOI: [10.1016/S0020-7683\(03\)00216-6](https://doi.org/10.1016/S0020-7683(03)00216-6).
- [14] W. Chen, and L. Wang, Large bending deformation of a cantilevered soft beam under external load: The applicability of inextensibility assumption of the centerline, *Cmm.*, vol. 1, no. 1, pp. 24–38, 2021. DOI: [10.2174/2666184501999200909151326](https://doi.org/10.2174/2666184501999200909151326).
- [15] L. A. Lubbers, M. van Hecke, and C. Coulais, A nonlinear beam model to describe the postbuckling of wide neo-hookean beams, *J. Mech. Phys. Solids* ., vol. 106, pp. 191–206, 2017. DOI: [10.1016/j.jmps.2017.06.001](https://doi.org/10.1016/j.jmps.2017.06.001).
- [16] Y. Chen, and L. Jin, Snapping-back buckling of wide hyperelastic columns, *Extreme Mech. Lett.*, vol. 34, pp. 100600, 2020. DOI: [10.1016/j.eml.2019.100600](https://doi.org/10.1016/j.eml.2019.100600).
- [17] I. D. Breslavsky, M. Amabili, and M. Legrand, Physically and geometrically non-linear vibrations of thin rectangular plates, *Int. J. Non. Linear Mech.*, vol. 58, pp. 30–40, 2014. DOI: [10.1016/j.ijnonlinmec.2013.08.009](https://doi.org/10.1016/j.ijnonlinmec.2013.08.009).
- [18] I. D. Breslavsky, M. Amabili, and M. Legrand, Nonlinear vibrations of thin hyperelastic plates, *J. Sound Vib.*, vol. 333, no. 19, pp. 4668–4681, 2014. DOI: [10.1016/j.jsv.2014.04.028](https://doi.org/10.1016/j.jsv.2014.04.028).
- [19] S. Aimmanee, and R. C. Batra, Analytical solution for vibration of an incompressible isotropic linear elastic rectangular plate, and frequencies missed in previous solutions, *J. Sound Vib.*, vol. 302, no. 3, pp. 613–620, 2007. DOI: [10.1016/j.jsv.2006.11.029](https://doi.org/10.1016/j.jsv.2006.11.029).
- [20] M. Amabili, P. Balasubramanian, I. D. Breslavsky, G. Ferrari, R. Garziera, and K. Riabova, Experimental and numerical study on vibrations and static deflection of a thin hyperelastic plate, *J. Sound Vib.*, vol. 385, pp. 81–92, 2016. DOI: [10.1016/j.jsv.2016.09.015](https://doi.org/10.1016/j.jsv.2016.09.015).
- [21] M. Amabili, I. D. Breslavsky, and J. N. Reddy, Nonlinear higher-order shell theory for incompressible biological hyperelastic materials, *Comput. Methods Appl. Mech. Eng.*, vol. 346, pp. 841–861, 2019. DOI: [10.1016/j.cma.2018.09.023](https://doi.org/10.1016/j.cma.2018.09.023).
- [22] J. P. Pascon, and H. B. Coda, A shell finite element formulation to analyze highly deformable rubber-like materials, *Lat. Am. J. Solids Struct.*, vol. 10, no. 6, pp. 1177–1209, 2013. DOI: [10.1590/S1679-78252013000600006](https://doi.org/10.1590/S1679-78252013000600006).
- [23] E. Carrera, M. Cinefra, M. Petrolo, and E. Zappino, *Finite Element Analysis of Structures through Unified Formulation*. John Wiley & Sons, Chichester, West Sussex, UK, 2014.
- [24] A. Pagani, and E. Carrera, Unified formulation of geometrically nonlinear refined beam theories, *Mech. Adv. Mater. Struct.*, vol. 25, no. 1, pp. 15–31, 2018. DOI: [10.1080/15376494.2016.1232458](https://doi.org/10.1080/15376494.2016.1232458).
- [25] B. Wu, A. Pagani, M. Filippi, W. Chen, and E. Carrera, Large-deflection and post-buckling analyses of isotropic rectangular plates by carrera unified formulation, *Int. J. Non. Linear Mech.*, vol. 116, pp. 18–31, 2019. DOI: [10.1016/j.ijnonlinmec.2019.05.004](https://doi.org/10.1016/j.ijnonlinmec.2019.05.004).
- [26] B. Wu, A. Pagani, W. Q. Chen, and E. Carrera, Geometrically nonlinear refined shell theories by Carrera unified formulation, *Mech. Adv. Mater. Struct.*, vol. 28, no. 16, pp. 1721–1741, 2021. DOI: [10.1080/15376494.2019.1702237](https://doi.org/10.1080/15376494.2019.1702237).
- [27] E. Carrera, A. Pagani, R. Azzara, and R. Augello, Vibration of metallic and composite shells in geometrical nonlinear equilibrium states, *Thin-Walled Struct.*, vol. 157, pp. 107131, 2020. DOI: [10.1016/j.tws.2020.107131](https://doi.org/10.1016/j.tws.2020.107131).
- [28] A. Pagani, and E. Carrera, Large-deflection and post-buckling analyses of laminated composite beams by carrera unified formulation, *Compos. Struct.*, vol. 170, pp. 40–52, 2017. DOI: [10.1016/j.compstruct.2017.03.008](https://doi.org/10.1016/j.compstruct.2017.03.008).
- [29] P. Flory, Thermodynamic relations for high elastic materials, *Trans. Faraday Soc.*, vol. 57, pp. 829–838, 1961. DOI: [10.1039/TF9615700829](https://doi.org/10.1039/TF9615700829).
- [30] E. Karabelas, G. Haase, G. Plank, and C. M. Augustin, Versatile stabilized finite element formulations for nearly and fully incompressible solid mechanics, *Comput. Mech.*, vol. 65, no. 1, pp. 193–215, 2020. DOI: [10.1007/s00466-019-01760-w](https://doi.org/10.1007/s00466-019-01760-w).
- [31] C. Wex, S. Arndt, A. Stoll, C. Bruns, and Y. Kupriyanova, Isotropic incompressible hyperelastic models for modelling the mechanical behaviour of biological tissues: A review, *Biomed. Eng./Biomedizinische Technik.*, vol. 60, no. 6, pp. 577–592, 2015.
- [32] L. R. G. Treloar, Stress-strain data for vulcanized rubber under various types of deformation, *Rubber Chem. Technol.*, vol. 17, no. 4, pp. 813–825, 1944. DOI: [10.5254/1.3546701](https://doi.org/10.5254/1.3546701).
- [33] A. N. Gent, A new constitutive relation for rubber, *Rubber Chem. Technol.*, vol. 69, no. 1, pp. 59–61, 1996. DOI: [10.5254/1.3538357](https://doi.org/10.5254/1.3538357).
- [34] H. Khajehsaeid, J. Arghavani, and R. Naghdabadi, A hyperelastic constitutive model for rubber-like materials, *Eur. J. Mech.-A/Solids.*, vol. 38, pp. 144–151, 2013. DOI: [10.1016/j.euromechsol.2012.09.010](https://doi.org/10.1016/j.euromechsol.2012.09.010).
- [35] H. Demiray, A note on the elasticity of soft biological tissues, *J. Biomech.*, vol. 5, no. 3, pp. 309–311, 1972. DOI: [10.1016/0021-9290\(72\)90047-4](https://doi.org/10.1016/0021-9290(72)90047-4).
- [36] C. Suchocki, A finite element implementation of Knowles stored-energy function: Theory, coding and applications, *Arch. Mech. Eng.*, vol. 58, no. 3, pp. 319–346, 2011. DOI: [10.2478/v10180-011-0021-7](https://doi.org/10.2478/v10180-011-0021-7).
- [37] G. A. Holzapfel, *Nonlinear Solid Mechanics: A Continuum Approach for Engineering*. John Wiley & Sons, Chichester, West Sussex, England, second print edition, 2001.
- [38] C. Suchocki, Finite element implementation of slightly compressible and incompressible first invariant-based hyperelasticity: Theory, coding, exemplary problems, *Jtam.*, vol. 55, pp. 787, 2017. DOI: [10.15632/jtam-pl.55.3.787](https://doi.org/10.15632/jtam-pl.55.3.787).
- [39] E. Carrera, G. Giunta, and M. Petrolo, *Beam Structures: Classical and Advanced Theories*. John Wiley & Sons, Chichester, West Sussex, England, 2011.
- [40] A. Pagani, and E. Carrera, Coupling three-dimensional peridynamics and high-order one-dimensional finite elements based on local elasticity for the linear static analysis of solid beams and thin-walled reinforced structures, *Int. J. Numer. Methods Eng.*, vol. 121, no. 22, pp. 5066–5081, 2020. DOI: [10.1002/nme.6510](https://doi.org/10.1002/nme.6510).
- [41] M. Filippi, A. Pagani, and E. Carrera, Accurate nonlinear dynamics and mode aberration of rotating blades, *J. Appl. Mech.*, vol. 85, no. 11, pp. 111004, 2018. DOI: [10.1115/1.4040693](https://doi.org/10.1115/1.4040693).
- [42] A. Pagani, R. Azzara, R. Augello, and E. Carrera, Stress states in highly flexible thin-walled composite structures by unified shell model, *AIAA J.*, vol. 59, no. 10, pp. 4243–4256, 2021. DOI: [10.2514/1.J060024](https://doi.org/10.2514/1.J060024).
- [43] A. Pagani, and A. R. Sanchez-Majano, Influence of fiber misalignments on buckling performance of variable stiffness composites using layerwise models and random fields, *Mech. Adv. Mater. Struct.*, 2020. DOI: [10.1080/15376494.2020.1771485](https://doi.org/10.1080/15376494.2020.1771485).
- [44] E. Carrera, and M. Petrolo, Refined beam elements with only displacement variables and plate/shell capabilities, *Meccanica.*, vol. 47, no. 3, pp. 537–556, 2012. DOI: [10.1007/s11012-011-9466-5](https://doi.org/10.1007/s11012-011-9466-5).
- [45] E. Carrera, A. Pagani, and R. Augello, Mul Group Large deflection and post-buckling of thin-walled structures by finite elements with node-dependent kinematics, *Acta Mech.*, vol. 232, no. 2, pp. 591–617, 2021. DOI: [10.1007/s00707-020-02857-7](https://doi.org/10.1007/s00707-020-02857-7).
- [46] M. A. Crisfield, *Non-Linear Finite Element Analysis of Solid and Structures*. John Wiley & Sons, Chichester, England, 1991.
- [47] J. N. Reddy, *An Introduction to Nonlinear Finite Element Analysis: With Applications to Heat Transfer, Fluid Mechanics, and Solid Mechanics*. Oxford University Press, Oxford, 2014.
- [48] M. A. Crisfield, A fast incremental/iterative solution procedure that handles “snap-through”, *Comput. Struct.*, vol. 13, no. 1-3, pp. 55–62, 1981. DOI: [10.1016/0045-7949\(81\)90108-5](https://doi.org/10.1016/0045-7949(81)90108-5).
- [49] M. A. Crisfield, An arc-length method including line searches and accelerations, *Int. J. Numer. Meth. Eng.*, vol. 19, no. 9, pp. 1269–1289, 1983. DOI: [10.1002/nme.1620190902](https://doi.org/10.1002/nme.1620190902).

- [50] E. Carrera, A study on arc-length-type methods and their operation failures illustrated by a simple model, *Comput. Struct.*, vol. 50, no. 2, pp. 217–229, 1994. DOI: [10.1016/0045-7949\(94\)90297-6](https://doi.org/10.1016/0045-7949(94)90297-6).
- [51] O. C. Zienkiewicz, and R. L. Taylor, *The Finite Element Method for Solid and Structural Mechanics*, 6th ed., Butterworth-Heinemann, Washington, 2005.
- [52] S. A. Maas, B. J. Ellis, G. A. Ateshian, and J. A. Weiss, FEBio: Finite elements for biomechanics, *J. Biomech. Eng.*, vol. 134, no. 1, pp. 011005, 2012.
- [53] S. Reese, P. Wriggers, and B. D. Reddy, A new locking-free brick element formulation for continuous large deformation problems, In *Computational Mechanics, New Trends and Applications*, Proceedings of the Fourth World Congress on Computational Mechanics WCCM IV Buenos Aires, CIMNE (Centro Internacional de Métodos Numéricos in Ingeniería), Barcelona, 1998.
- [54] T. Elguedj, Y. Bazilevs, V. M. Calo, and T. J. R. Hughes, \bar{B} and \bar{F} projection methods for nearly incompressible linear and non-linear elasticity and plasticity using higher-order nurbs elements, *Comput. Methods Appl. Mech. Eng.*, vol. 197, no. 33-40, pp. 2732–2762, 2008.
- [55] A. Masud, and T. J. Truster, A framework for residual-based stabilization of incompressible finite elasticity: Stabilized formulations and f methods for linear triangles and tetrahedra, *Comput. Methods Appl. Mech. Eng.*, vol. 267, pp. 359–399, 2013. DOI: [10.1016/j.cma.2013.08.010](https://doi.org/10.1016/j.cma.2013.08.010).
- [56] N. Büchter, E. Ramm, and D. Roehl, Three-dimensional extension of non-linear shell formulation based on the enhanced assumed strain concept, *Int. J. Numer. Meth. Eng.*, vol. 37, no. 15, pp. 2551–2568, 1994. DOI: [10.1002/nme.1620371504](https://doi.org/10.1002/nme.1620371504).